



OPEN

Aryl-quinoline-4-carbonyl hydrazone bearing different 2-methoxyphenoxyacetamides as potent α -glucosidase inhibitors; molecular dynamics, kinetic and structure–activity relationship studies

Haleh Hamedifar^{1,2}, Mahroo Mirfattahi³, Minoos Khalili Ghomi³, Homa Azizian⁴, Aida Iraj^{5,6}, Milad Noori⁷, Ali Moazzam³, Navid Dastyafteh⁷, Ali Nokhbehzaim⁸, Katayoun Mehrpour^{5,6}, Shahrzad Javanshir⁷, Somayeh Mojtavavi⁹, Mohammad Ali Faramarzi⁹, Bagher Larjani³, Mir Hamed Hajimiri¹⁰✉ & Mohammad Mahdavi³✉

Regarding the important role of α -glucosidase enzyme in the management of type 2 diabetes mellitus, the current study was established to design and synthesize aryl-quinoline-4-carbonyl hydrazone bearing different 2-methoxyphenoxyacetamide (11a–o) and the structure of all derivatives was confirmed through various techniques including IR, ¹H-NMR, ¹³C-NMR and elemental analysis. Next, the α -glucosidase inhibitory potentials of all derivatives were evaluated, and all compounds displayed potent inhibition with IC₅₀ values in the range of 26.0 ± 0.8–459.8 ± 1.5 μ M as compared to acarbose used as control, except 11f and 11l. Additionally, in silico-induced fit docking and molecular dynamics studies were performed to further investigate the interaction, orientation, and conformation of the newly synthesized compounds over the active site of α -glucosidase.

Nowadays, diabetes categorizes as the 6th cause of global mortality, and among different types of diabetes, type 2 diabetes mellitus (T2DM) accounts for 90% of the diabetic population, which has become a major health problem worldwide^{1,2}. Insulin is the hormone secreted by pancreatic β -cells and maintains glucose homeostasis by binding to cell receptors to transfer glucose. Also, insulin stimulates cells to get glucose from the blood and help the liver with glucose metabolism to lower glucose level to the normal condition³. Regarding the pathophysiology of T2DM, deficient insulin secretion by β -cells, tissue insulin resistance, and an inadequate compensatory insulin secretory response leads to high blood glucose level. This, in return associated with severe complications like, neuropathy, retinopathy, nephropathy, and cardiovascular problems⁴.

¹CinnaGen Medical Biotechnology Research Center, Alborz University of Medical Sciences, Karaj, Iran. ²CinnaGen Research and Production Co., Alborz, Iran. ³Endocrinology and Metabolism Research Center, Endocrinology and Metabolism Clinical Sciences Institute, Tehran University of Medical Sciences, Tehran, Iran. ⁴Department of Medicinal Chemistry, School of Pharmacy, Iran University of Medical Sciences, Tehran, Iran. ⁵Research Center for Traditional Medicine and History of Medicine, Department of Persian Medicine, School of Medicine, Shiraz University of Medical Sciences, Shiraz 7134845794, Iran. ⁶Stem Cells Technology Research Center, Shiraz University of Medical Sciences, Shiraz, Iran. ⁷Pharmaceutical and Heterocyclic Chemistry Research Laboratory, Department of Chemistry, Iran University of Science and Technology, Tehran 16846-13114, Iran. ⁸Student Research Committee, Alborz University of Medical Sciences, Karaj, Iran. ⁹Department of Pharmaceutical Biotechnology, Faculty of Pharmacy and Biotechnology Research Center, Tehran University of Medical Sciences, Tehran, Iran. ¹⁰Nano Alvand Company, Avicenna Tech Park, Tehran University of Medical Sciences, Tehran 1439955991, Iran. ✉email: h.hajimiri@nanoalvand.com; momahdavi@sina.tums.ac.ir

α -glucosidase (EC 3.2.1.20) is among the hydrolase group that attracted much attention due to its identification as a candidate for regulating blood glucose levels⁵. α -glucosidase hydrolyze 1,4- α -glucopyranosidic of oligosaccharide and disaccharide to produce monosaccharides contributing to the increase of glucose level. Acarbose, miglitol, and voglibose are commercially available α -glucosidase inhibitors; however, the routine consumption of these drugs is associated with bloating, diarrhea, and flatulence⁶. As a result, developing new α -glucosidase inhibitors is a valuable approach that slows down the catalytic activity of carbohydrates digestive enzyme⁷.

Heterocyclic compounds are an undeniable part of drug design, and amongst quinoline, as a heterocycle ring exhibited various pharmacological activities⁸. Also, functionalized quinoline moieties are essential pharmacophoric with various therapeutic properties as antimicrobial, anticancer, anti-inflammatory, antioxidant, and antidiabetic agents^{8,9}. The primary structure of quinoline (compounds **A** and **B**, Fig. 1) revealed good activity against α -glucosidase compared with the positive control acarbose ($IC_{50} = 66.5 \pm 1.5 \mu\text{g/mL}$). In previous work, we identified that introducing electron-donating groups and specious substitutions on compound **C** enhanced the inhibitory enzyme potential¹⁰. In another study, it was shown that compound **D** had higher inhibitory activity than positive control and exhibited selective and effective photodegrading ability against an α -glucosidase target upon photo-irradiation¹¹.

Schiff base derivatives are also present in some potent α -glucosidase inhibitors in these cases, compounds **E**, **F**, and **G**¹² are noble examples. The analysis of these derivatives reveals that this connecting group is critical for the interactions with the binding site of the enzyme and, consequently enzyme inhibition. The same is also evident in our previously reported series of cyanoacetohydrazide linked to 1,2,3-triazoles where the acetohydrazide linker is indeed a key structural feature governing their anti- α -glucosidase potency. Also, evaluation of the type of substitution on the phenoxy linker exhibited that methoxy substitution on the phenoxy linker significantly increased the activity¹³.

Arylacetamide derivatives have been developed and investigated as anti-diabetic agents. Diphenylimidazole core attached to the various N-aryl acetamides (Fig. 1, Compound **H**) were developed as α -glucosidase inhibitors with IC_{50} values of 25.2 to 176.5 μM compared with the standard inhibitor acarbose ($IC_{50} = 750.0 \mu\text{M}$). Compound **H** exhibited a competitive mode of inhibition with $K_i = 23 \mu\text{M}$ against α -glucosidase. In silico studies showed that the phenoxy linker of potent inhibitor exhibited H-bond interaction with Asp616 and/or Asp282^{14,15}. Also, compound **I** with benzimidazole-phenoxyacetamide structure was a competitive inhibitor of α -glucosidase with K_i of 67.0 μM with $45.0 \pm 0.8\%$ α -amylase inhibition at 108 μM ¹⁶. In 2022, quinazolin-4(3H)-one linked to phenoxy-acetamide derivatives (**J**) was synthesized and exhibited IC_{50} in the range of $14.4 \pm 0.2 \mu\text{M}$ to $> 750 \mu\text{M}$ was observed. In silico study showed phenoxy acetamide participated in several H-bond as well as hydrophobic

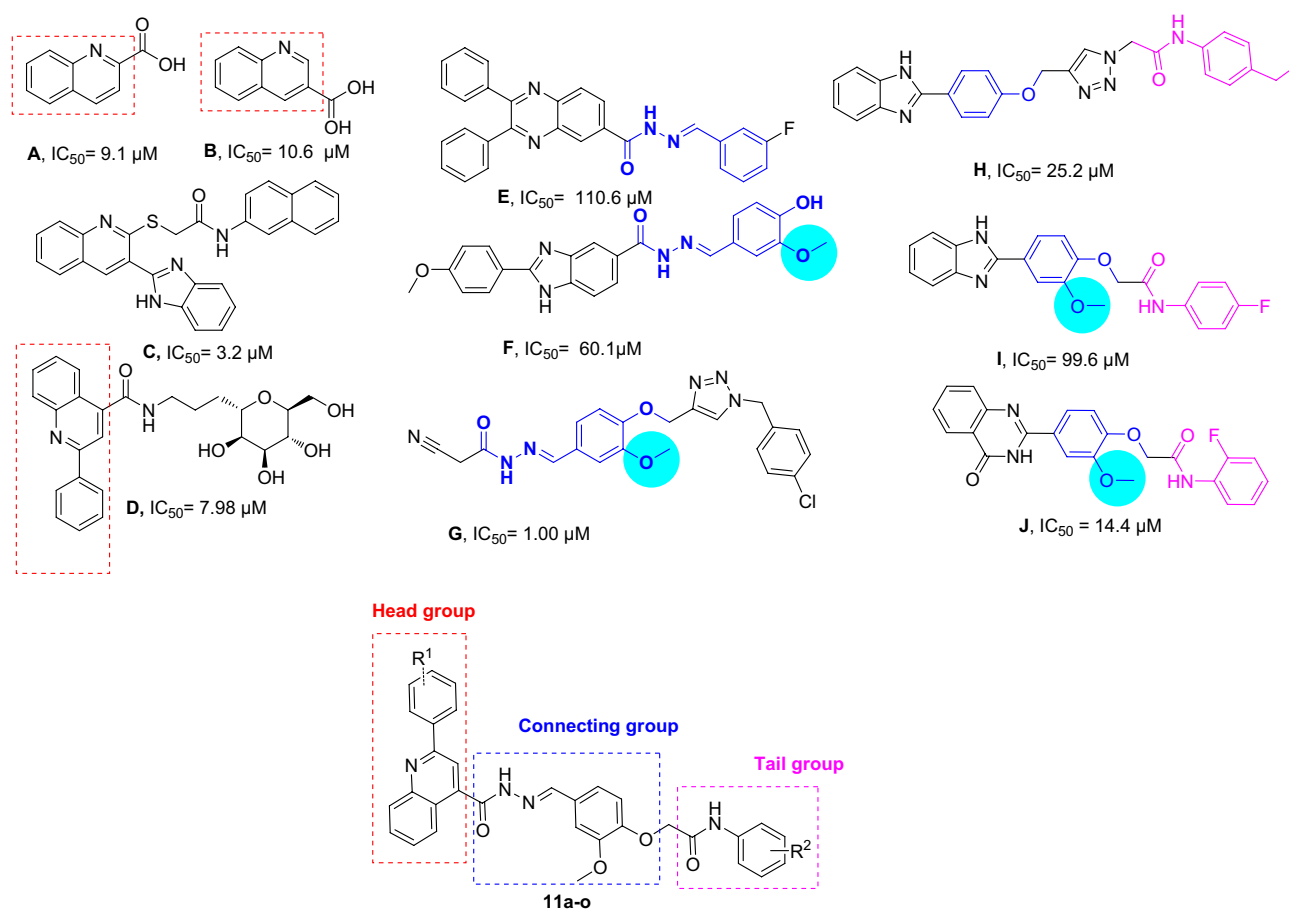


Figure 1. Demonstration of previously reported α -glucosidase inhibitors and designed compound.

interactions with Asp616, Arg600, and Trp48 of the enzyme active site¹⁷. Arylacetamide moiety seems to provide a suitable site for derivitization and proved to possess α -glucosidase inhibition.

Using a rational design of new molecules, we have chosen aryl-quinoline-4-carbonyl hydrazone conjugated to different 2-methoxyphenoxyacetamide moieties. The structure of all derivatives was confirmed with IR, ¹H-NMR, ¹³C-NMR, and elemental analysis. The synthesized derivatives were evaluated as α -glucosidase inhibitors, and the kinetic study of the most active analog was performed. Also, molecular dynamic studies of the most potent derivative were executed.

Results and discussion

Chemistry

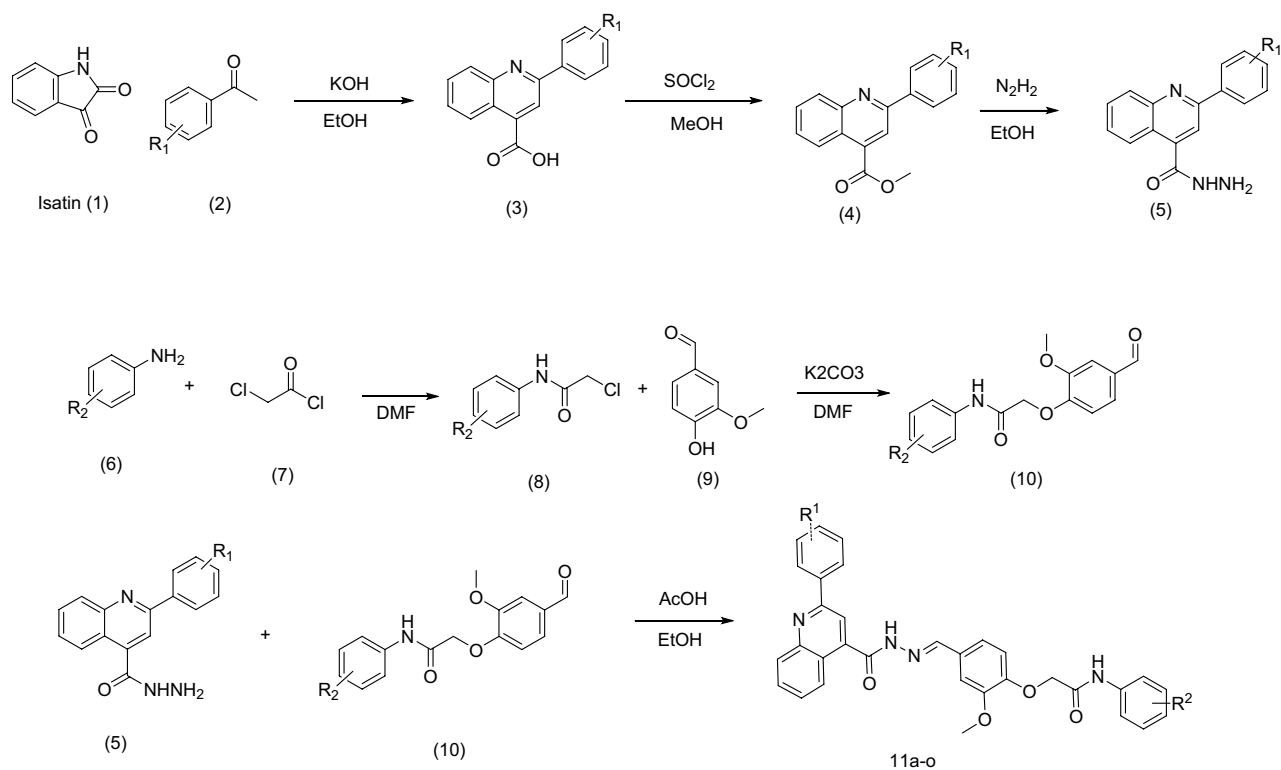
The synthesis of new aryl-quinoline-4-carbonyl hydrazone bearing different 2-methoxyphenoxyacetamide derivatives is presented in Scheme 1. Starting with commercially available isatin (1), substitutions with various commercially available acetophenone derivatives (2) afforded intermediaries (3). Additionally, 2-Aryl-quinoline-4-carboxylic acid (3) was suspended in SOCl₂ and after the 2 h, refluxed, and the mixture was cooled to 0 °C. Methanol was added to get the hydrochloride salt of methyl ester derivative (4). Subsequently, hydrazine hydrate in ethanol was added, and the mixture was refluxed to afford 5 derivatives. In the other reaction, aniline derivatives (6) were added to chloroacetylchloride (7) to get the. Next, 4-hydro-3-methoxy benzaldehyde was charged with 2-chloro-N-phenyl acetamide derivatives (8), followed by the addition of potassium carbonate to afford 10. Finally, hydrazone derivatives (5) were treated with the 2-(4-formyl-2-methoxyphenoxy)-N-aryl-acetamide derivatives (10) to provide the final products 11a–o. Synthesis details are given in the experimental section.

The NMR results confirmed the structures of all synthesized compounds, for example, in ¹H-NMR, individual peaks of the H group of –NH–N= appear in ~ 12 ppm, the H of NH group appears in ~ 10 ppm, H of N=CH appears in ~ 8.5 ppm. Also, the H of acetamide appears in around 5 ppm confirming the production of final products.

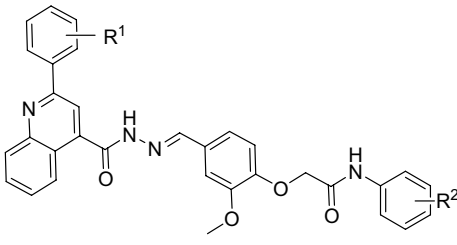
Biological evaluation and structure–activity relationships

The focused library of optimized 11a–o and their inhibitory potencies against α -glucosidase enzyme are presented in Table 1. To better evaluate the SARs, these analogs were divided into two categories based on the type of moiety at the R¹ position, 11a–g (R¹ = H), 11h–o (R¹ = OCH₃).

In the case of 11a–h, the methyl-containing derivatives (11a and 11b) improved the inhibition compared to the positive control, and the *ortho* position exhibited better potency *vs para* analog. The replacement of 4-methyl with a 4-methoxy moiety (11c) in general enhanced the potency compared with their methyl counterparts. Similarly, the *para* position recorded lower potency. Furthermore, an inhibitory effect of 11d was found to be IC₅₀ = 156.8 μ M, which contained a 4-ethyl substituent. It was understood that the increased bulkiness at



Scheme 1. Synthesis of the final compounds.



Compounds	R ¹	R ²	IC ₅₀ (μM)	Concentrations of precipitation (μM)
11a	H	2-CH ₃	34.8 ± 1.1	–
11b	H	4-CH ₃	95.2 ± 1.2	≥ 375
11c	H	4-OCH ₃	43.7 ± 1.0	–
11d	H	4-CH ₂ -CH ₃	156.8 ± 1.5	≥ 375
11e	H	4-F	52.6 ± 0.6	–
11f	H	4-Cl	> 750	≥ 375
11g	H	4-Br	180.9 ± 1.7	≥ 375
11h	OCH ₃	H	62.4 ± 0.9	≥ 375
11i	OCH ₃	2-CH ₃	71.2 ± 0.6	–
11j	OCH ₃	4-OCH ₃	61.8 ± 0.5	≥ 190
11k	OCH ₃	4-CH ₂ -CH ₃	26.0 ± 0.8	–
11l	OCH ₃	4-F	> 750	≥ 190
11m	OCH ₃	4-Br	152.2 ± 1.7	≥ 190
11n	OCH ₃	4-Cl	48.7 ± 0.9	≥ 190
11o	OCH ₃	4-NO ₂	459.8 ± 1.5	–
Acarbose	–	–	750.0 ± 2.0	–

Table 1. The α -glucosidase inhibition assay of **11a–o**. Data represented in terms of mean \pm SD.

the *para* position is not tolerated. Also, in most, the compounds encompassing halogen substitution showed the deterioration of the enzyme inhibition, and the best results came back to fluorine with a smaller size and strong electron-withdrawing power, followed by the bromine group. Unexpectedly *para*-chlorine substitution completely lost its potency.

To get more insight into the SARs properties, derivatives **11h–o** were synthesized bearing OCH₃ at R¹ position. **11h** derivatives as the unsubstituted analog of methoxy series exhibited an IC₅₀ value of 62.4 \pm 0.9 μ M, which is more than 11-fold more potent *vs* positive control. Subsequently, electron-donating groups on the phenyl ring were synthesized. **11i** bearing 2-CH₃ slightly reduced the potency compared while 4-OCH₃ substitution (**11j**) slightly improved the activity. Noteworthy replacement of methoxy moiety with 4-CH₂-CH₃ (**11k**) as bulk electron donating group resulting in the most potent derivative with IC₅₀ of 26.0 μ M. To test the electron-withdrawing properties at the R² position, we also synthesized **11l–o** derivatives. The inhibitory capability of these derivatives recorded a reduction in the potency and even the NO₂ moiety did not empower the activity in comparison with **11h** as an unsubstituted derivative. The exception in this trend came back to 4-Cl (**11n**) with an IC₅₀ value of 48.7 μ M.

In general, almost all of the reported compounds except **11f** and **11l** showed higher anti- α -glucosidase potency in comparison with the positive control. Also, a closer look at the results exhibited that series **11a–g** (R¹ = H), and **11h–o** (R¹ = OCH₃) demonstrated opposite results. 4-ethyl substitution of methoxy analogs (compound **11k**, R¹: OCH₃, R²: 4-CH₂-CH₃; IC₅₀ = 26.0 μ M) was the most potent derivative, while such substitution (**11d**) in the R¹ = H derivatives was one of the least active compounds. The same trend was seen between **11f** (R¹: H, R²: 4-Cl; IC₅₀ > 750 μ M) *vs* **11n** (R¹: 4-OCH₃, R²: 4-Cl; IC₅₀ = 48.7 μ M) as well as **11g** *vs* **11m**. This pinpoints that the type of substitution at the R¹ position is an issue; however, the impact of R² substitution seems to be even more significant, as already noted.

Overall, the intricate differences in inhibitory potencies among the synthesized compounds against α -glucosidase can be attributed to a combination of steric, electronic, and conformational effects introduced by the subtle substituent differences. A closer examination of the results revealed that the impact of R² substitution seemed more significant than that of R¹ substitution. Compound **11k**, with 4-ethyl substitution (R¹: OCH₃, R²: 4-CH₂-CH₃; IC₅₀ = 26.0 μ M), stood out as the most potent, emphasizing the importance of specific R² substitutions. The contrasting results between compounds **11f** and **11l**, as well as **11g** and **11m**, highlight that the type of substitution at the R¹ position plays a crucial role in the observed variations.

Enzyme kinetic studies

Based on the Lineweaver–Burk plot shown in Fig. 2a, it can be observed that the K_m (Michaelis–Menten constant) gradually increased while the V_{max} (maximum reaction rate) remained unchanged with increasing inhibitor

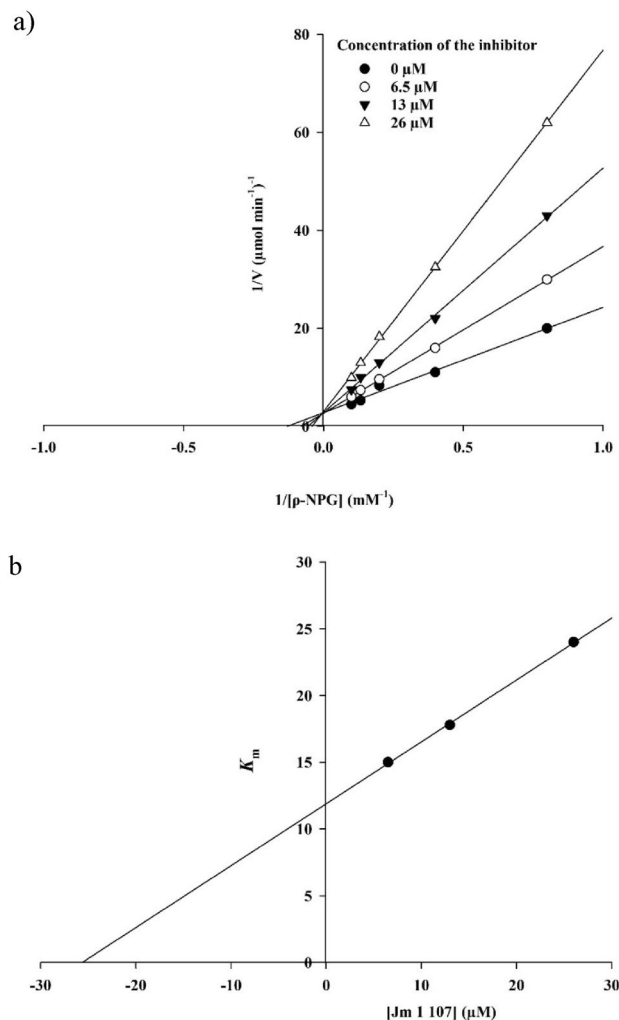


Figure 2. Kinetics of α -glucosidase inhibition by **11k**. (a) The Lineweaver–Burk plot in the absence and presence of different concentrations of **11k**; (b) The secondary plot between K_m and various concentrations of **11k**.

concentration. This pattern indicates a competitive inhibition mechanism. The results suggest that compound **11k** binds to the enzyme's active site and competes with the substrate for binding. Additionally, by plotting the K_m values against different inhibitor concentrations, an estimation of the inhibition constant (K_i) was obtained. The analysis yielded a K_i value of 25.6 μM , as depicted in Fig. 2b.

Docking study

A validated molecular docking procedure based on our previous studies was used to assess the binding mode of newly synthesized compounds **11a–o** and compare them with acarbose as the standard inhibitor of α -glucosidase. The reliability of the docking method was established by redocking the α -glucosidase natural substrate conducted by the previous study¹⁸.

Through previous investigation, the α -glucosidase active site is formed at the interface of domain A and domain B in which the residues from each side contribute to the active site region. In this way, phenylalanine residues play an important role at the entrance part of the active site. Furthermore, an active site lid is made up of residues 308–313, which plays an important role in substrate movement into the active site. Additionally, there are three conserved catalytic residues inside the active site pocket. They include Asp214 (nucleophile), Glu276 (general acid/base), and Asp 349, which stabilizes the substrate at the active site pocket¹⁹.

Figure 3 shows the interactions of acarbose in which the non-reducing end of acarbose (acarviosine moiety) is responsible for many important interactions with the enzyme. The valienamine moiety has hydrogen bonds to many residues in the –1 subsite, including: the conserved catalytic nucleophile, Asp214, and other residues like Asp68, Arg439, and His111. The protonated amino group interacts with Phe157 at the B domain through π -cation interaction. Also, at subsite, +1 acarviosine interacts with the conserved Asp349 through hydrogen bonds. By contrast, the reducing end of acarbose has several interactions with residues at the subsites +2 and +3 residues, including: Phe157, His239, Pro309, Arg312, Asp408, and Asn412.

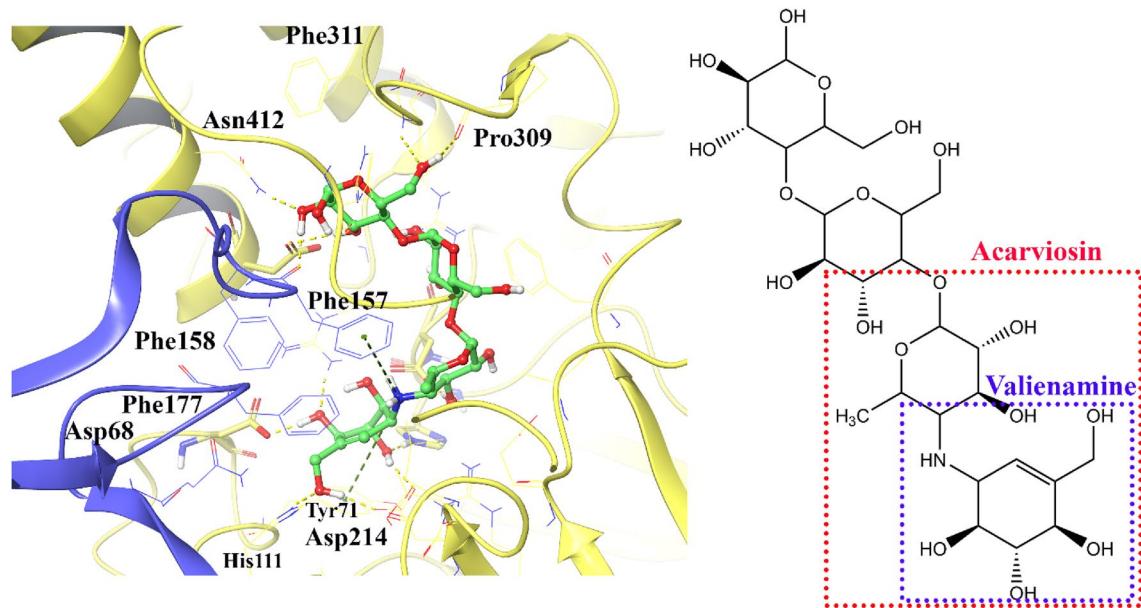


Figure 3. 3D representation of acarbose interaction at the α -glucosidase active site. The A domain of the α -glucosidase is depicted in yellow, and the B domain is shown in blue.

Figure 4a depicts the superimposed conformations and orientations of some of the synthesized compounds. It indicates that these compounds overall have similar conformations in which the 4-substituted acetanilide part of compounds oriented toward – 1 subsite is in the same position as the non-reducing end of acarbose (acarviosin moiety). Also, the quinoline nucleus provided the same orientation as the reducing part of acarbose through interaction at the active site mouth of the enzyme. Furthermore, Fig. 4b shows the non-bonding interactions of compound **11k**, as the best experimental active compound. The aromatic ring in the acetanilid moiety of the mentioned compound makes two π - π interactions with Phe298 and Tyr344. The aromatic ring in the dimethoxy benzene moiety makes a π - π interaction with Phe300 and an aromatic-hydrogen bond interaction with the conserved catalytic residue Asp349. Furthermore, the phenyl quinoline group interacts with Phe157, Ser308, Phe310, Arg312, and Asn412. The residues from 308 to 313 form the active site lid that plays an important role in substrate movement into the active site.

Molecular dynamic (MD) investigation

To study the stability of the dynamic behavior of the system, the best IFD pose of compound **11k** and acarbose were implemented as starting points for 100 ns MD simulation to predict the motion of complex systems at an atomistic level²⁰. Root mean square deviation (RMSD) values are indicative of the conformational stability and perturbations of the system. When RMSD values no longer follow a specific trend but fluctuate around a certain

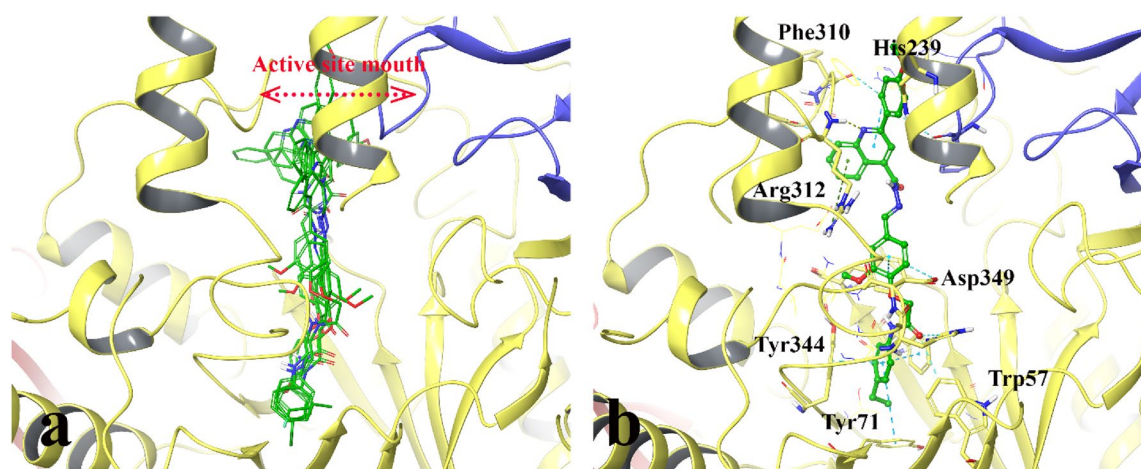


Figure 4. 3D poses of the docked structure of the synthesized compound over the α -glucosidase active site. The superimpose structure (a) and the IFD pose of the most promising compound, **11k** (b). The A domain of the α -glucosidase is depicted in yellow, and the B domain is shown in blue.

point, it can be argued that the complex has reached equilibrium²¹. Figure 5 depicts the protein backbone RMSD values for the α -glucosidase-**11k** complex (in green) and α -glucosidase-acarbose complex (in blue) over about 100 ns MD simulation time. The RMSD value of the α -glucosidase complexed with compound **11k** shows the same value as the enzyme complex with acarbose at the first 60 ns. Also, for the rest of the simulation time, the RMSDs plot became slightly increased and differentiative for both complexed systems in which it became a little lower for α -glucosidase-**11k** complex than acarbose one (about 1.75 Å and 2.1 Å, respectively). The such observation indicated that the employed simulation time was enough to obtain an equilibrium structure over the simulation time.

Furthermore, the 2D interactions diagram of compound **11k** in complex with the enzyme is depicted in Fig. 6. These interactions happened at least 30% duration of the MD simulation time. Figure 6 shows that the carbonyl oxygen of acetanilide moiety interacted with catalytic residues of Asp349 and Asp214 through water-mediated hydrogen bonds for about 42% and 39% of the simulation time, respectively. Also, at this part, the phenyl group stabilized through hydrophobic π - π stacking non-bonding interaction by His 348 and Tyr344 residues for about 30% of MD simulation time.

Also, the 2-methoxy phenyl quinoline moiety stabilized at the active site opening space through non-bonding interaction with Phe311 and Arg 312 for over half of the MD simulation time (51% and 62%, respectively). Moreover, the NH group belonging to the hydrazone provides water-mediated H-bond interaction with Glu304 for about 45% of MD simulation time. It is proved that the pose of compound **11k**, which resulted by the IFD investigation, is stable in that the acetanilide moiety is deeply inserted inside the active site pocket while the phenyl quinoline part is oriented between the entrance of the active site pocket.

In summary, through MD simulation investigation, it is revealed that the resulted in IFD posed of compound **11k** is stable at the α -glucosidase active pocket in which the 4-ethyl acetanilide part of compound **11k** oriented in -1 subsite which is in the same position as the non-reducing end of acarbose (acarviosine moiety) and is responsible for many important interactions through catalytic residue. Also, the 2-methoxy quinoline part provided the same orientation as the reducing part of acarbose through interaction at the active site mouth of the enzyme.

Conclusion

We describe the design and synthesis of aryl-quinoline-4-carbonyl hydrazone bearing different 2-methoxyphenoxacetamide compounds, and we have assessed the inhibitory effects of all compounds against α -glucosidase through in vitro assays. The results revealed that **11k** incorporating OCH₃ at R¹ and 4-CH₂-CH₃ at R² displayed the best inhibition potency against α -glucosidase with an IC₅₀ value of 26.0 ± 0.8 μ M. The SAR outcomes highlighted that the type of substitution at the R¹ position of phenyl-quinoline is important; however, the impact of R² substitution on acetamide seems to be even more significant effect, as already noted. Additionally, the kinetic investigation of **11k** as the most potent derivative offered the competitive type of α -glucosidase. Finally, an in silico study revealed that **11k** interacted with Glu304, Phe311, Arg312, Tyr344, His348, and Arg439 of the active site. These findings will be prominent for designing α -glucosidase inhibitors in drug discovery.

Experimental

General

All the reagents were purchased from commercial sources. ¹H and ¹³C NMR spectra were determined by a Bruker Advance spectrometer 400 MHz spectrometer. All the chemical shifts were reported as (δ) values ppm.

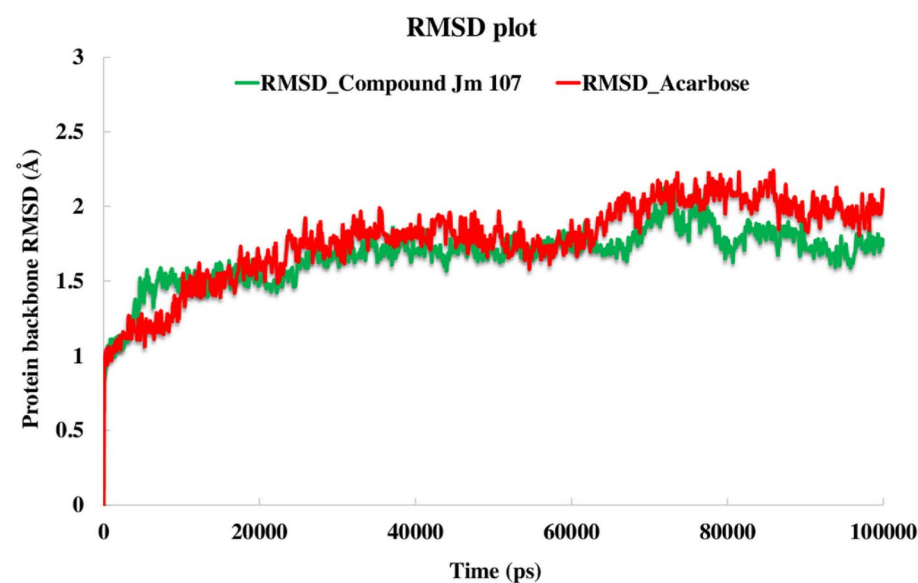


Figure 5. RMSD plot of α -glucosidase backbone in complex with acarbose (red) and compound **11k** (green), throughout the 100 ns of the simulation time.

Ligand-Protein Contacts

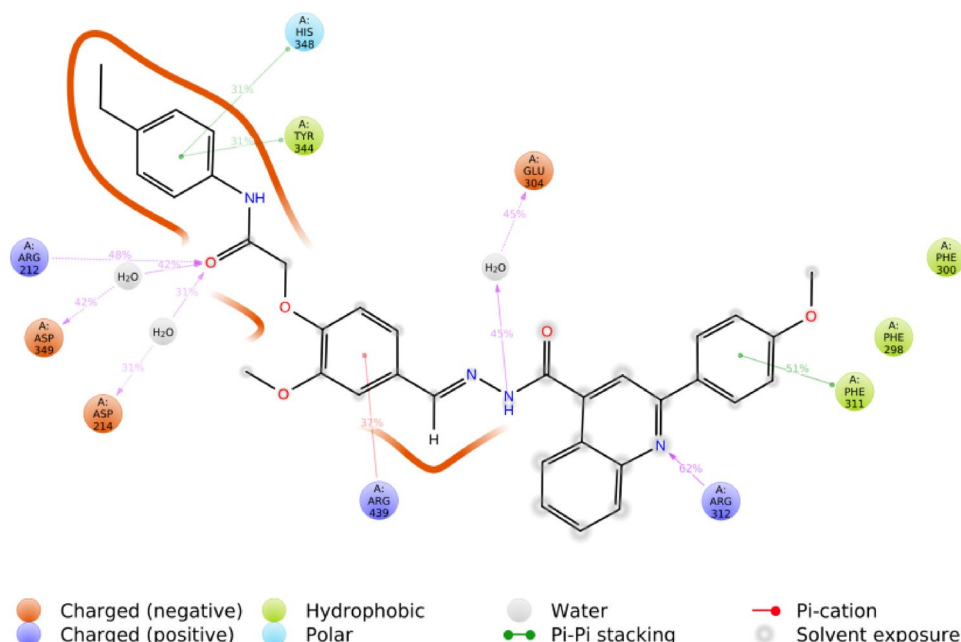


Figure 6. 2D interaction diagram of compound **11k**— α -glucosidase complex which is responsible for over 30% of MD simulation time.

Multiplicities were indicated by s (singlet), d (doublet), t (triplet), q (quartet), m (multiplet), and coupling constant J was reported in hertz (Hz). CHN analysis was performed using Costech Company. IR spectra were obtained with a Nicolet, FR-IR Magna 550. Melting points were also recorded using Kofler hot-stage apparatus. All the chemicals were purchased from Merck, Germany, and Sigma, Germany.

Synthesis

Synthesis of 2-aryl-quinoline-4-carboxylic acid derivatives (3)

Isatin (**1**, 13.66 mmol) was suspended in 55 mL of ethanol and heated to 65 °C to dissolve the solid. A solution of potassium hydroxide (33% w/v, 6.7 mL) was added and stirred at 65 °C for 15 min. Acetophenone derivatives (**2**, 15.4 mmol) were added dropwise to the heated solution. Upon complete addition, the reaction solution was warmed to reflux. After 48 h, the reaction solution was concentrated to a dark brown solid. A solution (60 mL) of 20% acetic acid in water was added slowly to adjust the pH to 5. The precipitate that formed was vacuum filtered and washed with EtOH and hexanes.

Synthesis of methyl 2-Aryl-quinoline-4-carboxylate derivatives (4)

2-Aryl-quinoline-4-carboxylic acid (**3**, 10 mmol) was suspended in SOCl_2 (12 mmol) at 0 °C. The mixture was refluxed for 2 h and cooled to 0 °C. Methanol (5 mL) was added to get the hydrochloride salt of the methyl ester derivative. Cold water (15 mL) was added to the mixture and its pH was adjusted to 7.0 with saturated with aqueous NaHCO_3 solution. The precipitated solid was filtered, washed with cold water (2 \times 10 mL), and dried under reduced pressure to get 2-(phenyl derivatives)-quinoline-4-carboxylic acid methyl ester.

Synthesis of methyl 2-Aryl-quinoline-4-carbohydrazide derivatives (5)

A mixture of methyl 2-arylquinoline-4-carboxylate and hydrazine hydrate (1 mL, 99%) in ethanol (10–15 mL) was refluxed for 10–14 h. After completion of the reaction, the reaction mixture was cooled to room temperature and poured into crushed ice. The white solid thus obtained was filtered, washed with water, and recrystallized from ethanol.

Synthesis of 2-chloro-N-aryl-acetamide derivatives (8)

Aniline derivatives (**6**, 1 mmol) were dissolved in DMF (4 mL), and then chloroacetylchloride (**7**, 1.2 mmol) was added at 0 °C. At room temperature, the mixture was stirred for 5 h, and subsequently poured into water, followed by filtration to isolate the desired product. The resulting solids were filtered, dried, and recrystallized from ethanol.

Synthesis of 2-(4-formyl-2-methoxyphenoxy)-N-aryl-acetamide derivatives (10)

To a solution of 4-hydro-3-methoxybenzaldehyde (9, 1 mmol) in DMF (5 mL), 2-chloro-N-phenylacetamide derivatives (8, 1.1 mmol) were added, followed by the addition of potassium carbonate (1.2 mmol). After stirring at room temperature for 5 h, the reaction mixture was poured into 25 mL of ice water. The resulting product was collected by filtration and rinsed with water.

Synthesis of 11a-o derivatives

4-substituted aldehyde (10, 1.1 mmol) and methyl 2-Aryl-quinoline-4-carbohydrazide derivatives (5, 1 mmol) and a few drops of glacial acetic acid as a catalyst in the absolute ethanol were refluxed for 6–7 h. The precipitate formed during the cooling of the mixture was filtered off, and washed two or three times with cold ethanol. Finally, the solid was recrystallized from ethanol (Supplementary Information).

2-(2-methoxy-4-((2-(2-phenylquinoline-4-carbonyl)hydrazineylidene)methyl)phenoxy)-N-(o-tolyl)acetamide (11a). Yield: 84%. Brown solid. M.p. > 250 °C. IR (KBr): 3422, 3105, 1676, 1558, 1342, 1175, 985 cm⁻¹. TLC (40:60; Hexane/AcOEt); R_f=0.48. ¹H NMR (400 MHz, DMSO-*d*₆) δ 12.21 (s, 1H, -NH-N=), 10.08 (s, 1H, NH), 8.39 (s, 1H, H_{Ar}), 8.38–8.35 (m, 2H, H_{Ar}), 8.34 (s, 1H, H_{Ar}), 8.25 (d, *J*=8.8 Hz, 2H, H_{Ar}), 8.19 (d, *J*=8.4 Hz, 1H, H_{Ar}), 7.87 (d, *J*=7.8 Hz, 1H, H_{Ar}), 7.69 (t, *J*=7.6 Hz, 1H, H_{Ar}), 7.59 (d, *J*=7.6 Hz, 2H, H_{Ar}), 7.57–7.51 (m, 4H, H_{Ar}), 7.53–7.45 (m, 1H, H_{Ar}), 7.26 (d, *J*=8.4 Hz, 1H, H_{Ar}), 7.14 (d, *J*=8.3 Hz, 2H, H_{Ar}), 7.06 (d, *J*=8.3 Hz, 1H, H_{Ar}), 4.79 (s, 2H, OCH₂), 3.92 (s, 3H, OCH₃), 2.26 (s, 3H, CH₃). ¹³C NMR (101 MHz, DMSO-*d*₆) δ 166.51, 163.18, 156.26, 150.12, 149.88, 149.25, 148.42, 141.90, 138.56, 136.37, 133.13, 130.85, 130.47, 130.14, 129.66, 129.42, 128.15, 127.82, 127.66, 125.63, 123.98, 122.49, 119.94, 117.72, 113.95, 109.27, 68.52, 56.09, 20.93. SI-MS (C₃₃H₂₈N₄O₄): calculated m/z 544.21 [M+H]⁺, observed m/z 544.32 [M+H]⁺; Anal. Calcd for C₃₃H₂₈N₄O₄: C, 72.78; H, 5.18; N, 10.29; Found: C 73.09; H 5.22; N 10.12.

2-(2-methoxy-4-((2-(2-phenylquinoline-4-carbonyl)hydrazono)methyl)phenoxy)-N-(p-tolyl)acetamide (11b). Yield: 81%. Brown solid. M.p. > 250 °C. IR (KBr): 3436, 3024, 1652, 1601, 1349, 1188 cm⁻¹. TLC (40:60; Hexane/AcOEt); R_f=0.44. ¹H NMR (400 MHz, DMSO-*d*₆) δ 12.21 (s, 1H, -NH-N=), 10.08 (s, 1H, NH), 8.39–8.34 (m, 4H, H_{Ar}), 8.25 (d, *J*=8.3 Hz, 1H, H_{Ar}), 8.19 (d, *J*=8.4 Hz, 1H, H_{Ar}), 7.90–7.83 (m, 1H, H_{Ar}), 7.72–7.66 (m, 1H, H_{Ar}), 7.61–7.51 (m, 5H, H_{Ar}), 7.49 (t, *J*=8.1 Hz, 1H, H_{Ar}), 7.26 (d, *J*=8.4 Hz, 1H, H_{Ar}), 7.14 (d, *J*=8.1 Hz, 2H, H_{Ar}), 7.06 (t, *J*=8.3 Hz, 1H, H_{Ar}), 4.79 (s, 2H, OCH₂), 3.91 (s, 3H, OCH₃), 2.26 (s, 3H, CH₃). ¹³C NMR (101 MHz, DMSO-*d*₆) δ 166.50, 163.17, 156.24, 150.10, 149.86, 149.24, 148.40, 141.88, 138.55, 136.36, 133.11, 130.83, 130.46, 130.13, 129.65, 129.40, 128.14, 127.90, 127.81, 125.62, 123.97, 122.48, 119.92, 117.71, 113.94, 109.26, 68.51, 56.09, 20.93. SI-MS (C₃₃H₂₈N₄O₄): calculated m/z 544.21 [M+H]⁺, observed m/z 544.27 [M+H]⁺; Anal. Calcd for C₃₃H₂₈N₄O₄: C 72.78; H 5.18; N 10.29; Found: C 72.63; H 5.01; N 10.44.

2-(2-methoxy-4-((2-(2-phenylquinoline-4-carbonyl)hydrazineylidene)methyl)phenoxy)-N-(4-methoxyphenyl)acetamide (11c). Yield: 84%. Brown solid. M.p. > 250 °C. IR (KBr): 3378, 3121, 1680, 1549, 1342, 1170, 989 cm⁻¹. TLC (40:60; Hexane/AcOEt); R_f=0.52. ¹H NMR (400 MHz, DMSO-*d*₆) δ 12.18 (s, 1H, -NH-N=), 10.02 (s, 1H, NH), 8.50–8.37 (m, 1H, H_{Ar}), 8.36 (s, 1H, H_{Ar}), 8.32 (d, *J*=7.8 Hz, 1H, H_{Ar}), 8.25 (d, *J*=8.2 Hz, 1H, H_{Ar}), 8.19 (d, *J*=8.3 Hz, 1H, H_{Ar}), 7.87 (d, *J*=8.4 Hz, 1H, H_{Ar}), 7.69 (d, *J*=8.6 Hz, 1H, H_{Ar}), 7.60 (d, *J*=8.6 Hz, 2H, H_{Ar}), 7.58–7.54 (m, 3H, H_{Ar}), 7.49–7.46 (m, 1H, H_{Ar}), 7.26 (d, *J*=8.3, 1H, H_{Ar}), 7.05 (d, *J*=8.4 Hz, 1H, H_{Ar}), 6.92 (d, *J*=8.9 Hz, 1H, H_{Ar}), 4.76 (s, 2H, OCH₂), 3.92 (s, 3H, OCH₃), 3.73 (s, 3H, OCH₃). ¹³C NMR (101 MHz, DMSO-*d*₆) δ 166.25, 163.13, 156.25, 155.98, 150.12, 149.87, 149.21, 148.40, 141.92, 138.55, 131.97, 130.86, 130.48, 130.13, 129.42, 127.81, 125.62, 122.47, 121.51, 114.39, 113.96, 109.26, 68.53, 56.10, 55.64. SI-MS (C₃₃H₂₈N₄O₅): calculated m/z 560.21 [M+H]⁺, observed m/z 560.23 [M+H]⁺; Anal. Calcd for C₃₃H₂₈N₄O₅: C, 70.70; H, 5.03; N, 9.99; Found: C 71.13; H 5.17; N 10.17.

N-(4-ethylphenyl)-2-(2-methoxy-4-((2-(2-phenylquinoline-4-carbonyl)hydrazono)methyl)phenoxy)acetamide (11d). Yield: 76%. Brown solid. M.p. > 250 °C. IR (KBr): 3419, 3074, 1659, 1623, 1357, 1169 cm⁻¹. TLC (40:60; Hexane/AcOEt); R_f=0.48. ¹H NMR (400 MHz, DMSO-*d*₆) δ 12.17 (s, 1H, -NH-N=), 10.08 (s, 1H, NH), 8.49–8.33 (m, 3H, H_{Ar}), 8.31 (s, 1H, H_{Ar}), 8.24 (d, *J*=8.3 Hz, 1H, H_{Ar}), 8.18 (d, *J*=8.2 Hz, 1H, H_{Ar}), 7.87 (d, *J*=8.4 Hz, 1H, H_{Ar}), 7.69 (d, *J*=8.3 Hz, 1H, H_{Ar}), 7.61–7.56 (m, 2H, H_{Ar}), 7.54 (d, *J*=8.7 Hz, 2H, H_{Ar}), 7.51–7.45 (m, 1H, H_{Ar}), 7.25 (d, *J*=9.1 Hz, 1H, H_{Ar}), 7.17 (d, *J*=8.4 Hz, 2H, H_{Ar}), 7.04 (d, *J*=8.3 Hz, 1H, H_{Ar}), 4.77 (s, 2H, OCH₂), 3.92 (s, 3H, OCH₃), 2.69–2.53 (m, 2H, CH₂Ethyl), 1.16 (t, *J*=7.6 Hz, 3H, CH₃Ethyl). ¹³C NMR (101 MHz, DMSO-*d*₆) δ 166.50, 163.11, 156.25, 150.09, 149.85, 148.39, 139.58, 138.54, 136.56, 130.87, 130.49, 129.43, 125.62, 123.96, 122.45, 119.99, 117.70, 113.92, 109.26, 68.46, 56.10, 28.08, 16.19. SI-MS (C₃₄H₃₀N₄O₄): calculated m/z 560.21 [M+H]⁺, observed m/z 560.29 [M+H]⁺; Anal. Calcd for C₃₄H₃₀N₄O₄: C, 73.10; H, 5.41; N, 10.03; O, 11.46; Found: C 73.54; H 5.47; N 10.09.

N-(4-fluorophenyl)-2-(2-methoxy-4-((2-(2-phenylquinoline-4-carbonyl)hydrazono)methyl)phenoxy)acetamide (11e). Yield: 79%. Brown solid. M.p. > 250 °C. IR (KBr): 3431, 3012, 1688, 1552, 1332, 1178, 925 cm⁻¹. TLC (40:60; Hexane/AcOEt); R_f=0.38. ¹H NMR (400 MHz, DMSO-*d*₆) δ 12.19 (s, 1H, -NH-N=), 10.24 (s, 1H, NH), 8.38–8.24 (m, 4H, H_{Ar}), 8.22 (d, *J*=8.4 Hz, 1H, H_{Ar}), 8.19 (d, *J*=8.3 Hz, 1H, H_{Ar}), 7.89–7.85 (m, 1H, H_{Ar}), 7.70–7.66 (m, 2H, H_{Ar}), 7.58–7.48 (m, 3H, H_{Ar}), 7.49 (d, *J*=8.1 Hz, 1H, H_{Ar}), 7.26 (d, *J*=8.4, 1H, H_{Ar}), 7.19 (t, *J*=8.9 Hz, 2H, H_{Ar}), 7.05 (d, *J*=8.3 Hz, 1H, H_{Ar}), 4.80 (s, 2H, OCH₂), 3.91 (s, 3H, OCH₃). ¹³C NMR (100 MHz, DMSO-*d*₆) δ 166.72, 163.15, 159.89 (¹J_{C-F}=239 Hz), 156.24, 150.05, 149.87, 149.21, 148.39, 141.89, 138.54, 135.27 (⁴J_{C-F}=2 Hz), 130.84, 130.47, 130.13, 129.41, 128.18, 127.91, 127.80, 125.61, 123.96, 122.46, 121.81

($^3J_{C-F} = 8 \text{ Hz}$), 117.70, 115.97 ($^2J_{C-F} = 22 \text{ Hz}$), 113.97, 109.27, 68.45, 56.08. SI-MS ($C_{32}H_{25}FN_4O_4$): calculated m/z 548.57 $[M+H]^+$, observed m/z 548.60 $[M+H]^+$; *Anal. Calcd* for $C_{32}H_{25}FN_4O_4$: C 70.06; H 4.59; N 10.21; Found: C 69.89; H 4.47; N 10.02.

N-(4-chlorophenyl)-2-(2-methoxy-4-((2-(2-phenylquinoline-4-carbonyl)hydrazono)methyl)phenoxy)acetamide (11f). Yield: 71%. Brown solid. M.p. > 250 °C. IR (KBr): 3443, 3031, 1684, 1587, 1324, 1206, 736 cm^{-1} . TLC (40:60; Hexane/AcOEt); $R_f = 0.48$. 1H NMR (400 MHz, DMSO- d_6) δ 12.27 (s, 1H, -NH-N=), 10.42 (s, 1H, NH), 8.43–8.29 (m, 4H, H_{Ar}), 8.21 (d, $J = 8.5 \text{ Hz}$, 2H, H_{Ar}), 7.87 (t, $J = 7.8 \text{ Hz}$, 1H, H_{Ar}), 7.70–7.55 (m, 6H, H_{Ar}), 7.47 (t, $J = 7.9 \text{ Hz}$, 1H, H_{Ar}), 7.40 (d, $J = 8.5 \text{ Hz}$, 2H, H_{Ar}), 7.25 (d, $J = 8.2 \text{ Hz}$, 1H, H_{Ar}), 7.04 (d, $J = 8.3 \text{ Hz}$, 1H, H_{Ar}), 4.81 (s, 2H, OCH_2), 3.91 (s, 3H, OCH_3). ^{13}C NMR (101 MHz, DMSO- d_6) δ 166.97, 163.15, 156.24, 150.02, 149.84, 149.21, 148.38, 141.90, 138.55, 137.89, 130.83, 130.46, 130.12, 129.41, 129.18, 128.18, 127.90, 127.80, 127.69, 125.62, 123.96, 122.44, 121.49, 117.71, 113.92, 109.26, 68.38, 56.09. SI-MS ($C_{32}H_{25}ClN_4O_4$): calculated m/z 565.03 $[M+H]^+$, observed m/z 565.05 $[M+H]^+$; *Anal. Calcd* for $C_{32}H_{25}ClN_4O_4$: C 68.02; H 4.46; N 9.29; Found: C 67.88; H 4.23; N 9.11.

N-(4-bromophenyl)-2-(2-methoxy-4-((2-(2-phenylquinoline-4-carbonyl)hydrazineylidene)methyl)phenoxy)acetamide (11g). Yield: 74%. Brown solid. M.p. > 250 °C. IR (KBr): 3451, 3018, 1677, 1563, 1320, 1192, 668 cm^{-1} . TLC (40:60; Hexane/AcOEt); $R_f = 0.39$. 1H NMR (400 MHz, DMSO- d_6) δ 12.25 (s, 1H, -NH-N=), 10.39 (s, 1H, NH), 8.38–8.18 (m, 6H, H_{Ar}), 7.86 (t, $J = 7.9 \text{ Hz}$, 1H, H_{Ar}), 7.70–7.48 (m, 9H, H_{Ar}), 7.25 (d, $J = 8.2 \text{ Hz}$, 1H, H_{Ar}), 7.05 (d, $J = 8.2 \text{ Hz}$, 1H, H_{Ar}), 4.82 (s, 2H, OCH_2), 3.91 (s, 3H, OCH_3). ^{13}C NMR (101 MHz, DMSO- d_6) δ 167.00, 163.17, 156.23, 150.03, 149.84, 149.23, 148.40, 141.87, 138.55, 138.30, 132.09, 130.82, 130.46, 130.13, 129.40, 128.18, 127.89, 127.80, 125.63, 123.97, 122.46, 121.87, 117.72, 115.76, 113.93, 109.25, 68.41, 56.08. SI-MS ($C_{32}H_{25}BrN_4O_4$): calculated m/z 609.48 $[M+H]^+$, observed m/z 609.51 $[M+H]^+$; *Anal. Calcd* for $C_{32}H_{25}BrN_4O_4$: C 63.06; H 4.13; N 9.19; Found: C 62.85; H 4.31; N 9.39.

2-(2-methoxy-4-((2-(2-(4-methoxyphenyl)quinoline-4-carbonyl)hydrazono)methyl)phenoxy)-N-phenylacetamide (11h). Yield: 71%. Brown solid. M.p. > 250 °C. IR (KBr): 3453, 3027, 1660, 1585, 1344, 1229 cm^{-1} . TLC (40:60; Hexane/AcOEt); $R_f = 0.50$. 1H NMR (400 MHz, DMSO- d_6) δ 12.27 (s, 1H, -NH-N=), 10.24 (s, 1H, NH), 8.36–8.30 (m, 4H, H_{Ar}), 8.21 (d, $J = 8.4 \text{ Hz}$, 1H, H_{Ar}), 8.14 (d, $J = 8.4 \text{ Hz}$, 1H, H_{Ar}), 7.83 (t, $J = 7.6 \text{ Hz}$, 1H, H_{Ar}), 7.66 (d, $J = 7.4 \text{ Hz}$, 2H, H_{Ar}), 7.49 (d, $J = 8.8 \text{ Hz}$, 1H, H_{Ar}), 7.40–7.29 (m, 2H, H_{Ar}), 7.25 (d, $J = 8.3 \text{ Hz}$, 1H, H_{Ar}), 7.15–7.04 (m, 5H, H_{Ar}), 4.82 (s, 2H, OCH_2), 3.89 (m, 6H, $2 \times OCH_3$). ^{13}C NMR (101 MHz, DMSO- d_6) δ 166.76, 163.31, 161.38, 155.89, 150.06, 149.84, 149.19, 148.39, 141.78, 138.91, 130.98, 130.69, 129.89, 129.29, 129.22, 128.17, 127.39, 125.59, 124.13, 123.63, 122.46, 119.90, 117.21, 114.76, 113.88, 109.22, 68.43, 56.08, 55.80. SI-MS ($C_{33}H_{28}N_4O_5$): calculated m/z 560.61 $[M+H]^+$, observed m/z 560.64 $[M+H]^+$; *Anal. Calcd* for $C_{33}H_{28}N_4O_5$: C 70.70; H 5.03; N 9.99; Found: C 70.52; H 5.21; N 10.18.

2-(2-methoxy-4-((2-(2-(4-methoxyphenyl)quinoline-4-carbonyl)hydrazono)methyl)phenoxy)-N-(o-tolyl)acetamide (11i). Yield: 71%. Brown solid. M.p. > 250 °C. IR (KBr): 3439, 3011, 1648, 1575, 1328, 1164 cm^{-1} . TLC (40:60; Hexane/AcOEt); $R_f = 0.45$. 1H NMR (400 MHz, DMSO- d_6) δ 12.27 (s, 1H, -NH-N=), 9.43 (s, 1H, NH), 8.36–8.06 (m, 6H, H_{Ar}), 7.83 (t, $J = 7.9 \text{ Hz}$, 1H, H_{Ar}), 7.71–7.38 (m, 3H, H_{Ar}), 7.34–7.01 (m, 7H, H_{Ar}), 4.84 (s, 2H, OCH_2), 3.92 (s, 3H, OCH_3), 3.87 (s, 3H, OCH_3), 2.24 (s, 3H, CH_3). ^{13}C NMR (101 MHz, DMSO- d_6) δ 166.71, 163.29, 161.39, 155.89, 149.82, 149.73, 149.12, 148.38, 141.81, 136.02, 131.25, 130.98, 130.85, 130.79, 130.70, 129.29, 128.30, 127.40, 126.62, 125.69, 125.59, 124.38, 123.63, 122.34, 117.20, 114.77, 113.92, 109.28, 68.24, 56.14, 55.82, 17.96. SI-MS ($C_{34}H_{30}N_4O_5$): calculated m/z 574.640 $[M+H]^+$, observed m/z 574.66 $[M+H]^+$; *Anal. Calcd* for $C_{34}H_{30}N_4O_5$: C 71.07; H 5.26; N 9.75; Found: C 70.90; H 5.46; N 9.58.

2-(2-methoxy-4-((2-(2-(4-methoxyphenyl)quinoline-4-carbonyl)hydrazono)methyl)phenoxy)-N-(4-methoxyphenyl)acetamide (11j). Yield: 76%. Brown solid. M.p. > 250 °C. IR (KBr): 3458, 3025, 1638, 1581, 1326, 1212 cm^{-1} . TLC (40:60; Hexane/AcOEt); $R_f = 0.58$. 1H NMR (400 MHz, DMSO- d_6) δ 12.17 (s, 1H, -NH-N=), 10.02 (s, 1H, NH), 8.36–8.30 (m, 3H, H_{Ar}), 8.18 (d, $J = 8.2 \text{ Hz}$, 1H, H_{Ar}), 8.13 (d, $J = 8.4 \text{ Hz}$, 1H, H_{Ar}), 7.83 (t, $J = 8.00 \text{ Hz}$, 1H, H_{Ar}), 7.64 (t, $J = 7.5 \text{ Hz}$, 1H, H_{Ar}), 7.55 (d, $J = 8.9 \text{ Hz}$, 2H, H_{Ar}), 7.47 (d, $J = 8.2 \text{ Hz}$, 1H, H_{Ar}), 7.25 (d, $J = 8.4 \text{ Hz}$, 1H, H_{Ar}), 7.14 (d, $J = 8.8 \text{ Hz}$, 2H, H_{Ar}), 7.05 (d, $J = 8.3 \text{ Hz}$, 1H, H_{Ar}), 6.92 (d, $J = 8.7 \text{ Hz}$, 2H, H_{Ar}), 4.76 (s, 2H, OCH_2), 3.91 (s, 3H, OCH_3), 3.87 (s, 3H, OCH_3), 3.73 (s, 3H, OCH_3). ^{13}C NMR (101 MHz, DMSO- d_6) δ 166.24, 163.22, 161.39, 155.96, 155.88, 150.08, 149.85, 149.13, 148.37, 141.77, 131.96, 130.96, 130.72, 129.89, 129.29, 129.13, 128.14, 127.42, 125.56, 123.60, 122.43, 121.49, 117.18, 114.77, 114.38, 109.24, 68.50, 56.09, 55.82, 55.64. SI-MS ($C_{34}H_{30}N_4O_6$): calculated m/z 590.64 $[M+H]^+$, observed m/z 590.61 $[M+H]^+$; *Anal. Calcd* for $C_{34}H_{30}N_4O_6$: C 69.14; H 5.12; N 9.49; Found: C 68.96; H 4.91; N 9.67.

N-(4-ethylphenyl)-2-(2-methoxy-4-((2-(2-(4-methoxyphenyl)quinoline-4-carbonyl)hydrazono)methyl)phenoxy)acetamide (11k). Yield: 68%. Brown solid. M.p. > 250 °C. IR (KBr): 3446, 3014, 1657, 1593, 1335, 1183 cm^{-1} . TLC (40:60; Hexane/AcOEt); $R_f = 0.51$. 1H NMR (400 MHz, DMSO- d_6) δ 12.18 (s, 1H, -NH-N=), 10.08 (s, 1H, NH), 8.36–8.30 (m, 4H, N=CH, H_3 , $H_{2,6}$), 8.20 (d, $J = 8.2 \text{ Hz}$, 1H, H_5), 8.14 (d, $J = 8.4 \text{ Hz}$, 1H, H_8), 7.83 (t, $J = 7.8 \text{ Hz}$, 1H, H_7), 7.64 (t, $J = 7.6 \text{ Hz}$, 1H, H_6), 7.56 (d, $J = 8.3 \text{ Hz}$, 2H, $H_{2,6}$ acetamide), 7.49 (s, 1H, $H_{2,7}$), 7.26 (d, $J = 8.2 \text{ Hz}$, 1H, $H_{6,7}$), 7.18–7.13 (m, 4H, $H_{3,5}$ acetamide, $H_{3,5,7}$), 7.05 (d, $J = 8.3 \text{ Hz}$, 1H, $H_{5,7}$), 4.79 (s, 2H, CH_{2} acetamide), 3.91 (s, 3H, OCH_3), 3.86 (s, 3H, OCH_3), 2.56 (q, $J = 7.6 \text{ Hz}$, 2H, CH_{2} Ethyl), 1.16 (t, $J = 7.6 \text{ Hz}$, 3H, CH_3 Ethyl). ^{13}C NMR (101 MHz, DMSO- d_6) δ 166.51, 163.25, 161.39, 155.89, 150.08, 149.85, 149.16, 148.39, 141.74, 139.59, 136.54, 130.97, 130.71, 129.29, 128.47, 128.15, 127.41, 125.56, 123.61, 122.45, 120.00, 119.96, 117.19, 114.77, 113.92,

109.24, 68.49, 56.08, 55.80, 28.09, 16.18. SI-MS ($C_{35}H_{32}N_4O_5$): calculated m/z 588.24 $[M+H]^+$, observed m/z 588.45 $[M+H]^+$; Anal. Calcd for $C_{35}H_{32}N_4O_5$: C 71.41; H 5.48; N 9.52; Found: C 71.21; H 5.66; N 9.34.

N-(4-fluorophenyl)-2-(2-methoxy-4-((2-(2-(4-methoxyphenyl)quinoline-4-carbonyl)hydrazono)methyl)phenoxy)acetamide (11l). Yield: 83%. Brown solid. M.p. > 250 °C. IR (KBr): 3455, 3039, 1674, 1603, 1341, 1175, 991 cm^{-1} . TLC (40:60; Hexane/AcOEt); $R_f=0.54$. 1H NMR (400 MHz, DMSO- d_6) δ 12.19 (s, 1H, -NH-N=), 10.25 (s, 1H, NH), 8.36–8.32 (m, 4H, H_{Ar}), 8.20 (d, $J=8.7$ Hz, 1H, H_{Ar}), 8.14 (d, $J=8.4$ Hz, 1H, H_{Ar}), 7.84 (t, $J=8.1$ Hz, 1H, H_{Ar}), 7.70–7.62 (m, 3H, H_{Ar}), 7.49 (d, $J=8.2$ Hz, 1H, H_{Ar}), 7.26 (d, $J=8.3$ Hz, 1H, H_{Ar}), 7.21–7.13 (m, 4H, H_{Ar}), 7.05 (d, $J=8.3$ Hz, 1H, H_{Ar}), 4.80 (s, 2H, OCH_2), 3.89 (m, 6H, $2 \times OCH_3$). ^{13}C NMR (101 MHz, DMSO- d_6) δ 166.73, 163.26, 161.39, 159.89 ($^1J_{C-F}=239$ Hz), 155.88, 150.03, 149.85, 149.15, 148.39, 141.74, 135.28 ($^4J_{C-F}=3$ Hz), 130.96, 130.71, 129.90, 129.29, 128.18, 127.42, 125.56, 123.61, 122.45, 121.80 ($^3J_{C-F}=8$ Hz), 117.19, 115.97 ($^2J_{C-F}=22$ Hz), 114.76, 113.94, 109.23, 68.43, 56.07, 55.80. SI-MS ($C_{33}H_{27}FN_4O_5$): calculated m/z 578.60 $[M+H]^+$, observed m/z 578.63 $[M+H]^+$; Anal. Calcd for $C_{33}H_{27}FN_4O_5$: C 68.50; H 4.70; N 9.68; Found: C 68.35; H 4.57; N 9.42.

N-(4-bromophenyl)-2-(2-methoxy-4-((2-(2-(4-methoxyphenyl)quinoline-4-carbonyl)hydrazono)methyl)phenoxy)acetamide (11m). Yield: 79%. Brown solid. M.p. > 250 °C. IR (KBr): 3462, 3030, 1669, 1579, 1338, 1223, 652 cm^{-1} . TLC (40:60; Hexane/AcOEt); $R_f=0.49$. 1H NMR (400 MHz, DMSO- d_6) δ 12.21 (s, 1H, -NH-N=), 10.36 (s, 1H, NH), 8.36–8.81 (m, 4H, H_{Ar}), 8.20 (d, $J=8.1$ Hz, 1H, H_{Ar}), 8.13 (d, $J=8.3$ Hz, 1H, H_{Ar}), 7.82 (t, $J=8.0$ Hz, 1H, H_{Ar}), 7.66–7.62 (m, 3H, H_{Ar}), 7.53 (d, $J=8.7$ Hz, 2H, H_{Ar}), 7.48 (d, $J=8.5$ Hz, 1H, H_{Ar}), 7.25 (d, $J=8.4$ Hz, 1H, H_{Ar}), 7.14 (d, $J=8.7$ Hz, 2H, H_{Ar}), 7.04 (d, $J=8.3$ Hz, 1H, H_{Ar}), 4.81 (s, 2H, OCH_2), 3.91 (s, 3H, OCH_3), 3.86 (s, 3H, OCH_3). ^{13}C NMR (101 MHz, DMSO- d_6) δ 166.99, 163.25, 161.39, 155.88, 150.00, 149.84, 149.15, 148.39, 141.74, 138.28, 132.10, 130.96, 130.70, 129.89, 129.29, 128.20, 127.41, 125.57, 123.61, 122.43, 121.86, 117.19, 115.76, 114.77, 113.94, 109.26, 68.42, 56.08, 55.81. SI-MS ($C_{33}H_{28}BrN_4O_5$): calculated m/z 639.51 $[M+H]^+$, observed m/z 639.55 $[M+H]^+$; Anal. Calcd for $C_{33}H_{27}BrN_4O_5$: C 61.98; H 4.26; N 8.76; Found: C 61.77; H 4.38; N 8.59.

N-(4-chlorophenyl)-2-(2-methoxy-4-((2-(2-(4-methoxyphenyl)quinoline-4-carbonyl)hydrazono)methyl)phenoxy)acetamide (11n). Yield: 81%. Brown solid. M.p. > 250 °C. IR (KBr): 3449, 3022, 1675, 1594, 1346, 1219 cm^{-1} . TLC (40:60; Hexane/AcOEt); $R_f=0.54$. 1H NMR (400 MHz, DMSO- d_6) δ 12.19 (s, 1H, -NH-N=), 10.33 (s, 1H, NH), 8.36–8.31 (m, 4H, H_{Ar}), 8.20 (d, $J=8.2$ Hz, 1H, H_{Ar}), 8.14 (d, $J=8.3$ Hz, 1H, H_{Ar}), 7.83 (t, $J=8.1$ Hz, 1H, H_{Ar}), 7.70–7.61 (m, 3H, H_{Ar}), 7.48 (d, $J=8.2$ Hz, 1H, H_{Ar}), 7.40 (d, $J=8.6$ Hz, 2H, H_{Ar}), 7.25 (d, $J=8.3$ Hz, 1H, H_{Ar}), 7.14 (d, $J=8.8$ Hz, 2H, H_{Ar}), 7.05 (d, $J=8.3$ Hz, 1H, H_{Ar}), 4.81 (s, 2H, OCH_2), 3.91–3.86 (m, 6H, $2 \times OCH_3$). ^{13}C NMR (101 MHz, DMSO- d_6) δ 166.97, 163.25, 161.39, 155.88, 150.01, 149.85, 149.14, 148.39, 141.75, 137.85, 130.96, 130.71, 129.90, 129.29, 129.19, 128.20, 127.73, 127.41, 125.56, 123.61, 122.43, 121.49, 117.19, 114.77, 113.95, 109.27, 68.42, 56.08, 55.80. SI-MS ($C_{33}H_{27}ClN_4O_5$): calculated m/z 595.05 $[M+H]^+$, observed m/z 595.07 $[M+H]^+$; Anal. Calcd for $C_{33}H_{27}ClN_4O_5$: C 66.61; H 4.57; N 9.42; Found: C 66.33; H 4.29; N 9.24.

2-(2-methoxy-4-((2-(2-(4-methoxyphenyl)quinoline-4-carbonyl)hydrazono)methyl)phenoxy)-N-(4-nitrophenyl)acetamide (11o). Yield: 77%. Yellow solid. M.p. > 250 °C. IR (KBr): 3456, 3016, 1691, 1552, 1351, 1234 cm^{-1} . TLC (40:60; Hexane/AcOEt); $R_f=0.32$. 1H NMR (400 MHz, DMSO- d_6) δ 12.24 (s, 1H, -NH-N=), 9.59 (s, 1H, NH), 8.36–8.30 (m, 4H, H_{Ar}), 8.22–8.12 (m, 4H, H_{Ar}), 8.13 (d, $J=8.4$ Hz, 1H, H_{Ar}), 7.85 (t, $J=7.8$ Hz, 1H, H_{Ar}), 7.65 (t, $J=7.6$ Hz, 1H, H_{Ar}), 7.51 (s, 1H, H_{Ar}), 7.31 (d, $J=8.3$ Hz, 1H, H_{Ar}), 7.24 (d, $J=8.9$ Hz, 2H, H_{Ar}), 7.17–7.13 (m, 3H, H_{Ar}), 5.05 (s, 2H, OCH_2), 3.99 (s, 3H, OCH_3), 3.87 (s, 3H, OCH_3). ^{13}C NMR (101 MHz, DMSO- d_6) δ 166.31, 163.39, 161.40, 155.88, 149.72, 148.87, 148.37, 148.02, 145.08, 143.12, 141.82, 138.88, 130.94, 130.74, 129.90, 129.29, 128.29, 127.45, 126.37, 125.52, 123.57, 121.83, 117.19, 115.80, 114.78, 108.43, 67.79, 56.50, 55.82. SI-MS ($C_{33}H_{27}N_5O_7$): calculated m/z 605.60 $[M+H]^+$, observed m/z 605.63 $[M+H]^+$; Anal. Calcd for $C_{33}H_{27}N_5O_7$: C 65.45; H 4.49; N 11.56; Found: C 65.22; H 4.71; N 11.33.

α -glucosidase inhibition assay

The anti- α -glucosidase effects of synthesized compounds were screened according to the previously reported method^{22,23}.

Enzyme kinetic studies

The mode of inhibition of the most potent derivative **11k**, identified with the lowest IC_{50} , was investigated against an α -glucosidase activity at different concentrations of substrate, *p*-nitrophenyl α -D-glucopyranoside (1–10 mM), as in the absence and presence of **11k** at different concentrations (0, 6.5, 13, and 26 μ M) as reported in our pressures^{12,14,24}.

Molecular dynamic (MD) simulation

In this study, the molecular dynamics (MD) simulation was carried out using the Desmond v5.3 module, which is integrated into the Maestro interface from Schrodinger 2018-4 suite²⁴. The IFD method was used to obtain the appropriate pose for the MD simulation procedure of the compounds²⁵. In order to conduct MD simulation, the first step involved solvating the protein–ligand complexes with explicit SPC water molecules and positioning them at the center of an appropriately sized orthorhombic box under Periodic Boundary Condition. To mimic real cellular ionic concentrations, counterions and a 0.15 M solution of NaCl were added to neutralize the system. The MD protocol consisted of three steps: minimization, pre-production, and production MD simulations.

The system was allowed to relax for 2500 steps by the steepest descent approach to minimize the energy. Next, a small force constant was applied to the enzyme as the system's temperature was gradually raised from 0 to 300 K to prevent abrupt changes. MD simulations were executed under the NPT (constant number of atoms, constant pressure—1.01325 bar, and constant temperature—300 K) ensemble, utilizing the Nose–Hoover chain method as the default. Long-range electrostatic forces were calculated using the Particle-mesh-based Ewald approach, with a cutoff radius for Columbia forces set to 9.0 Å. The protein–ligand complex underwent 100 ns of production MD simulations, with data frames stored every 1000 ps during the simulation. The dynamic behavior and structural changes of the systems were analyzed by the calculation of the root mean square deviation (RMSD) and interaction diagram (Supplementary Information).

Data availability

All data generated or analysed during this study are included in this published article.

Received: 5 May 2023; Accepted: 19 December 2023

Published online: 03 January 2024

References

- Mirzaei, M., Rahmanian, M., Mirzaei, M., Nadjarzadeh, A. & Dehghani Tafti, A. A. Epidemiology of diabetes mellitus, pre-diabetes, undiagnosed and uncontrolled diabetes in Central Iran: Results from Yazd health study. *BMC Public Health* **20**, 166 (2020).
- Reed, J., Bain, S. & Kanamarlapudi, V. A review of current trends with type 2 diabetes epidemiology, aetiology, pathogenesis, treatments and future perspectives. *Diabetes Metab. Syndr. Obes.* **14**, 3567–3602 (2021).
- Galicia-Garcia, U. *et al.* Pathophysiology of type 2 diabetes mellitus. *Int. J. Mol. Sci.* **21**, 6275 (2020).
- Mohammadi-Khanapostani, M. *et al.* Synthesis, α -glucosidase inhibition, in silico pharmacokinetic, and docking studies of thieno[2,3-*b*]quinoline-acetamide derivatives as new anti-diabetic agents. *ChemistrySelect* **7**, e202104482 (2022).
- Noori, M. *et al.* Design, synthesis, in vitro, and in silico enzymatic evaluations of thieno[2,3-*b*]quinoline-hydrazones as novel inhibitors for α -glucosidase. *Bioorganic Chem.* **127**, 105996 (2022).
- Fallah, Z. *et al.* A review on synthesis, mechanism of action, and structure-activity relationships of 1,2,3-triazole-based α -glucosidase inhibitors as promising anti-diabetic agents. *J. Mol. Struct.* **1255**, 132469 (2022).
- Niri, D. R. *et al.* Design, synthesis, in vitro, and in silico biological evaluations of coumarin-indole hybrids as new anti- α -glucosidase agents. *BMC Chem.* **16**, 84 (2022).
- Ajani, O. O., Iyaye, K. T. & Ademosun, O. T. Recent advances in chemistry and therapeutic potential of functionalized quinoline motifs—A review. *RSC Adv.* **12**, 18594–18614 (2022).
- Tabassum, R., Ashfaq, M. & Oku, H. Current pharmaceutical aspects of synthetic quinoline derivatives. *Mini Rev. Med. Chem.* **21**, 1152–1172 (2021).
- Noori, M. *et al.* Design, synthesis, and in silico studies of quinoline-based-benzo[d]imidazole bearing different acetamide derivatives as potent α -glucosidase inhibitors. *Sci. Rep.* **12**, 14019 (2022).
- Kitamura, T., Okuyama, M., Takahashi, D. & Toshima, K. 2-Phenylquinoline–sugar hybrids as photoswitchable α -glucosidase inhibitors. *Chemistry* **14**, 1409–1412 (2019).
- Azizian, H. *et al.* Docking study, molecular dynamic, synthesis, anti- α -glucosidase assessment, and ADMET prediction of new benzimidazole-Schiff base derivatives. *Sci. Rep.* **12**, 14870 (2022).
- Iraji, A. *et al.* Cyanoacetohydrazide linked to 1,2,3-triazole derivatives: A new class of α -glucosidase inhibitors. *Sci. Rep.* **12**, 8647 (2022).
- Asemanipoor, N. *et al.* Synthesis and biological evaluation of new benzimidazole-1,2,3-triazole hybrids as potential α -glucosidase inhibitors. *Bioorganic Chem.* **95**, 103482 (2020).
- Sepehri, N. *et al.* New 4, 5-diphenylimidazole-acetamide-1,2,3-triazole hybrids as potent α -glucosidase inhibitors: Synthesis, in vitro and in silico enzymatic and toxicity evaluations. *Monatshefte für Chemie-Chem. Mon.* **152**, 679–693 (2021).
- Shayegan, N. *et al.* Design, synthesis, and in silico studies of benzimidazole bearing phenoxyacetamide derivatives as α -glucosidase and α -amylase inhibitors. *J. Mol. Struct.* **1268**, 133650 (2022).
- Moheb, M. *et al.* Synthesis and bioactivities evaluation of quinazolin-4(3H)-one derivatives as α -glucosidase inhibitors. *BMC Chem.* **16**, 97 (2022).
- Azimi, F. *et al.* Design, synthesis, biological evaluation, and molecular modeling studies of pyrazole-benzofuran hybrids as new α -glucosidase inhibitor. *Sci. Rep.* **11**, 20776 (2021).
- Sherafati, M. *et al.* Quinazolinone-dihydropyran[3,2-*b*]pyran hybrids as new α -glucosidase inhibitors: Design, synthesis, enzymatic inhibition, docking study and prediction of pharmacokinetic. *Bioorg. Chem.* **109**, 104703 (2021).
- Hollingsworth, S. A. & Dror, R. O. Molecular dynamics simulation for all. *Neuron* **99**, 1129–1143 (2018).
- Grossfield, A. & Zuckerman, D. M. Quantifying uncertainty and sampling quality in biomolecular simulations. *Annu. Rep. Comput. Chem.* **5**, 23–48 (2009).
- Nikookar, H. *et al.* Design, synthesis and in vitro α -glucosidase inhibition of novel dihydropyran[3,2-*c*]quinoline derivatives as potential anti-diabetic agents. *Bioorganic Chem.* **77**, 280–286 (2018).
- Saeedi, M. *et al.* Design and synthesis of novel quinazolinone-1,2,3-triazole hybrids as new anti-diabetic agents: In vitro α -glucosidase inhibition, kinetic, and docking study. *Bioorganic Chem.* **83**, 161–169 (2019).
- Adib, M. *et al.* New 6-amino-pyrido[2,3-*d*]pyrimidine-2,4-diones as novel agents to treat type 2 diabetes: A simple and efficient synthesis, α -glucosidase inhibition, molecular modeling and kinetic study. *Eur. J. Med. Chem.* **155**, 353–363 (2018).
- Ivanova, L. *et al.* Molecular dynamics simulations of the interactions between glial cell line-derived neurotrophic factor family receptor GFR α 1 and small-molecule ligands. *ACS Omega* **3**, 11407–11414 (2018).

Author contributions

H.H., M.M., M.K.G., M.N., N.D., A.M. and S.J synthesized compounds and contributed to the characterization of compounds. A. N., S.M., M.A.F., and B.L. performed biological tests. H.A., A.I., K.M performed in silico study and contributed to the manuscript preparation. M.H.H. and M.M. supervised all phases of the study.

Competing interests

The authors declare no competing interests.

Additional information

Supplementary Information The online version contains supplementary material available at <https://doi.org/10.1038/s41598-023-50395-8>.

Correspondence and requests for materials should be addressed to M.H.H. or M.M.

Reprints and permissions information is available at www.nature.com/reprints.

Publisher's note Springer Nature remains neutral with regard to jurisdictional claims in published maps and institutional affiliations.



Open Access This article is licensed under a Creative Commons Attribution 4.0 International License, which permits use, sharing, adaptation, distribution and reproduction in any medium or format, as long as you give appropriate credit to the original author(s) and the source, provide a link to the Creative Commons licence, and indicate if changes were made. The images or other third party material in this article are included in the article's Creative Commons licence, unless indicated otherwise in a credit line to the material. If material is not included in the article's Creative Commons licence and your intended use is not permitted by statutory regulation or exceeds the permitted use, you will need to obtain permission directly from the copyright holder. To view a copy of this licence, visit <http://creativecommons.org/licenses/by/4.0/>.

© The Author(s) 2024